Research Article

Junling Wang, Yongbo Zhang*, Xiao Yang*, and Xiaobing Ma

Stress effect on 3D culturing of MC3T3-E1 cells on microporous bovine bone slices

https://doi.org/10.1515/ntrev-2020-0103
received November 23, 2020; accepted December 1, 2020

Abstract: The choosing of micromechanical environment is very important for the growth of bone-related cells. In this paper, bovine cancellous bone slices with 3D porous structures were used for 3D culturing of MC3T3-E1 cells (Mouse embryo osteoblast precursor cells) through a four-point-bending device due to their good biocompatibility and strength. Effects of micromechanical environment on the growth of MC3TC-E1 cells were investigated by immunofluorescent staining and alkaline phosphatase analysis, and the most positive microporous structures were found. In addition, a model of cell density vs stress was established through a specific normalization method and finite element simulation. The results showed that the micromechanical environment of the bone slices promoted cell proliferation, and the detail influence of stress on cell proliferation could be described by the mathematical model, which could provide a theoretical basis for the design of micromechanical environment in the bone tissue engineering scaffolds to stimulate cell proliferation.

Keywords: microporous structures, stress effect, MC3T3-E1 cells, 3D culturing, finite element simulation, mathematical model

*** Corresponding author: Yongbo Zhang,** Research Center of Small Sample Technology, School of Aeronautic Science and Engineering, Beihang University, Beijing, 100191, China; Aircraft and Propulsion Laboratory, Ningbo Institute of Technology, Beihang University, Ningbo, 315100, China, e-mail: zhangyongbo@buaa.edu.cn
*** Corresponding author: Xiao Yang,** Key Laboratory for Biomechanics and Mechanobiology of Ministry of Education, Beijing Advanced Innovation Center for Biomedical Engineering, School of Biological Science and Medical Engineering, Beihang University, Beijing, 100191, China, e-mail: xiaoyang@buaa.edu.cn
Junling Wang, Xiaobing Ma: School of Reliability and System Engineering, Beihang University, Beijing, 100191, China

1 Introduction

Large bone defects caused by various reasons, such as traffic accidents or diseases, are hard to heal without surgery [1]. Worldwide, more than 2 million bone-grafting procedures are performed every year, occupying a market value for bone grafts and substitute materials of approximately 2.7 billion dollars globally [2]. Common options for bone defect treatment include autogenous bone grafting and allogeneic bone grafting, both of which have their own limitations. Autograft is the gold standard for bone grafting. However, due to the insufficient supply, autograft is only suitable to repair small bone defects, and it is prone to cause iatrogenic injury, postoperative pain, and other complications [3]. Although allograft has a less limited supply compared to autograft, it also has problems such as poor osteoinductive capacity, risk of postoperative fracture, and immune rejection. Nowadays, nanotechnology and various advanced materials began to be widely used in the diagnosis and treatment of diseases, such as biosensors, drug delivery system, tissue engineering scaffolds, etc. [4–7]. In this context, bone tissue engineering technology emerges and provides a new solution for the treatment of bone defects. Tissue engineering scaffolds usually have complex microporous structures to provide more adherent area for cells. After the tissue engineering scaffold with living cells and growth factors is implanted into the defect site, the scaffold degrades gradually and the cells continuously proliferate and differentiate to form new bone tissue to repair the defect in the body [8]. Bone tissue engineering has abundant graft sources and good application prospects. It could potentially be widely used in the field of bone defect repair in the future.

Tissues and cells *in vivo* are believed to be subjected to mechanical load and respond accordingly during activities of daily life. For example, bone is understood to adaptively change its structure and density in response to changes in external loads [9,10]. However, residual stresses and strains, which are those that exist when all external loads are removed, are also found to be ubiquitous in the tissues and organs of organisms and may play

an important role [11–13]. For instance, circumferential compressive residual strains in the arteries are believed to effectively reduce the stretching of blood pressure and the risk of arterial rupture [14,15]. Similarly, residual stresses have also been measured in the bones [16–19] and may be important for maintaining their growth and structure. However, current research on tissue engineering scaffolds mainly focuses on the fabrication method and their interaction with microenvironments *in vivo* [20,21], while ignoring the effect of stress in the tissue engineering scaffolds on the bone repair process. As cell is the basic unit of life activity, it is the basis to study the effect of stress on cells in cell-level. Therefore, it is of significance to study cell responses to stress in tissue engineering scaffolds. If the effect of the stress on cell growth can be figured out and a stress environment that is conducive to cell growth can be introduced in the tissue engineering scaffolds, achieving rapid proliferation and differentiation of osteoblasts and formation of new bone, it may bring tremendous innovation to the bone tissue engineering technology.

There have been a lot of studies about the influence of stress on cells, and the results show that different loading methods, loading size, loading frequency, and loading time will have different effects on the proliferation, differentiation, and gene expression of cells cultured *in vitro* [22–26]. However, most of the research mentioned above is performed on a 2D (two-dimensional) plane, which cannot simulate the conditions most cells experience *in vivo*, because cells are living as a monolayer on a flat surface [27,28]. In addition, the conclusions obtained in previous studies are almost qualitative, and there is no quantitative model about the effect of stress on cells to determine the most appropriate stress to simulate cells, which brings difficulties to translate correlative research results into clinical application in the process of bone defect repair.

Although there is little theory established regarding the effect of stress on cell growth currently, the theory of bone remodeling has developed for a long time, which quantitatively describes the physiological behavior that the density of bone tissue changes with the change of mechanical environment [29,30]. Generally, in the areas with low loads, the mass and density of the bone will decrease, and in the areas with high loads, the mass and density of the bone will increase. Ref. [31] has improved the model which considered that excessively high loads will also cause a decrease in mass and density of the bone, and the process can be described by

$$\mathrm{d}M/\mathrm{d}t = B(U - k) - D(U - k)^2 \tag{1}$$

where B and D are the proportionality coefficients, M is the density of the bone, U is the mechanical excitation, which could be stress, strain, or strain energy density, etc. k is the reference excitation, t is time.

When the excitation is small, the first term on the right side of the equation plays the main role and the bone density increases; when the load is large, the quadratic term plays the main role and the bone density decreases. The theory of bone remodeling provides a reference for this paper to build the numerical model of the effect of stress on cell growth.

As is introduced above, bone defect diseases are very common around the world currently, while the repairing methods have various limitations and new breakthroughs in treatment methods are urgently needed. Bone tissue engineering scaffolds seem to be a promising solution to this problem, but it is not yet mature enough to be used for clinical application. Previous research has showed that the mechanical load has certain effects on the formation of new bone macroscopically and cellular life activities microscopically [22–26,32]. Based on this fact, figuring out the effect of the micromechanical environment of porous tissue engineering scaffolds on the process of bone defect repair, which is hardly considered in the current research, will greatly promote their application in the bone defect treatment field. As a basis, this paper studied the effect of stress on cell growth in the microporous bone slices which were similar to the tissue engineering scaffolds.

MC3T3-E1 cell, a kind of pre-osteoblast cell line, which has the capacity to differentiate into osteoblasts [33], was used in this study to investigate the effect of stress on their proliferation and activity in the microporous structures. Bovine cancellous bones have good biocompatibility and relatively high strength, which can usually withstand larger loads. Therefore, microporous bone slices were obtained from bovine cancellous bones to perform 3D (three-dimensional) cell culture experiments. Stress in the porous structure was simulated through four-point bending which is similar to residual stress measured in bovine bones. Ultimately, the differences in cell proliferation and viability between the stressed and control groups were compared. Based on the experimental results, mathematical model of the effect of stress on cell proliferation was established, preliminarily obtaining the effect of different magnitudes of stress on cell proliferation in the microporous structures.

2 Materials and methods

2.1 Bone slices

Microporous bone slices were used to provide a 3D living environment for cells. To obtain suitable bone slices, the metaphyses of fresh bovine femurs were cut using an electric saw, during which uneven areas such as soft tissues and growth plates were removed, obtaining approximate cuboid bone blocks. Subsequently, the bone blocks were cut with a precise cutter into pieces of 40 × 10 × 1.2 mm^3. To eliminate the grease in the bone slices, they were immersed in the 30% hydrogen peroxide solution (Beijing Chemical Works, China) and placed in an ultrasonic cleaner. After 3–5 days, they were taken out and rinsed under distilled water. This whole procedure was repeated until the solution became clear and the voids of the bone slices were evident, as shown in Figure 1. The bone slices were then washed 5 times with 1× PBS and sterilized in 4× AB/AM (antibiotic/antimycotic) solution (Genview, USA) diluted with distilled water for 2 days with the AB/AM changed once. Subsequently, the bone slices were incubated in DMEM (Gibco, USA) for 1 day, which was repeated two times until the medium color was stable. The treated bone slices were stored at −20°C for further use.

The microstructure morphology of the bone slice was observed under a SEM (Scanning electron microscope). The results showed that it had complex microporous structures with high porosity. The pore size was approximately between 100 and 900 μm, as shown in Figure 2.

2.2 Loading device

A custom-made four-point bending device was designed to create a stress environment in the bone slices, which is shown in Figure 3. It consists of a customized cell culture dish made of Teflon and aluminum alloy indenters inside (Figure 3d). The lid and bottom of the culture dish are tightly connected to the upper and lower indenter, respectively (Figure 3b and c).

Figure 1: The configuration of the bone slice after degreasing.

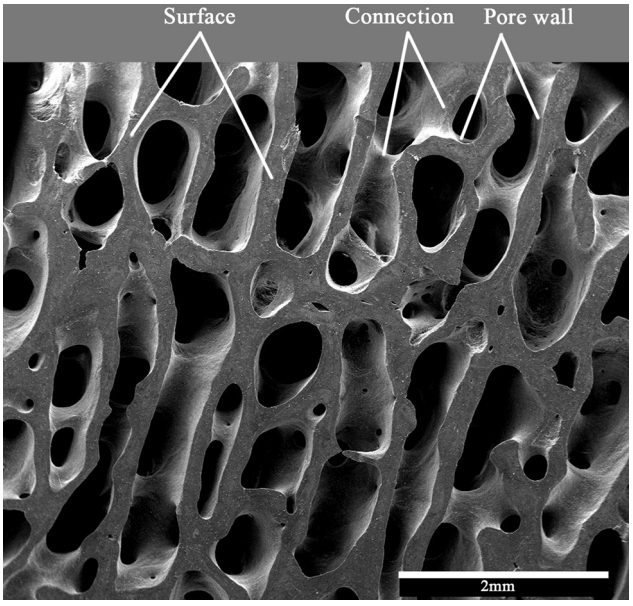

Figure 2: The microstructure morphology of the bone slice under SEM and the structures are divided into three typical structures.

After placing the bone slice with living cells into the device, weights were placed on the lid to create a bending moment in the bone slice. The part of the bone slice between the two fulcrums of the lower indenter was in a pure bending state. According to the theory of mechanics of materials, the maximum bending moment in the bone slice M_{max} is given by

$$M_{max} = (m_0 + m)g(L - L_0)/8 \quad (2)$$

where M_{max} is maximum bending moment in the bone slice, m_0 is the quality of the lid and the upper indenter, m is the quality of weights, L is the distance between the two fulcrums of the lower indenter, L_0 is the distance between the two fulcrums of the upper indenter, and g is the gravitational acceleration. The key parameters of the loading device are as follows: $m_0 = 22.64$ g, $m = 20$ g, $L = 32$ mm, $L_0 = 22$ mm.

Cells on the bone slice were subjected to bending stress. If the bone slice was treated as a homogeneous material, the maximum bending stress can be expressed as

$$\sigma = 6M_{max}/bh^2 \quad (3)$$

where σ is bending stress, b is the width of the bone slice, and h is the height of the bone slice.

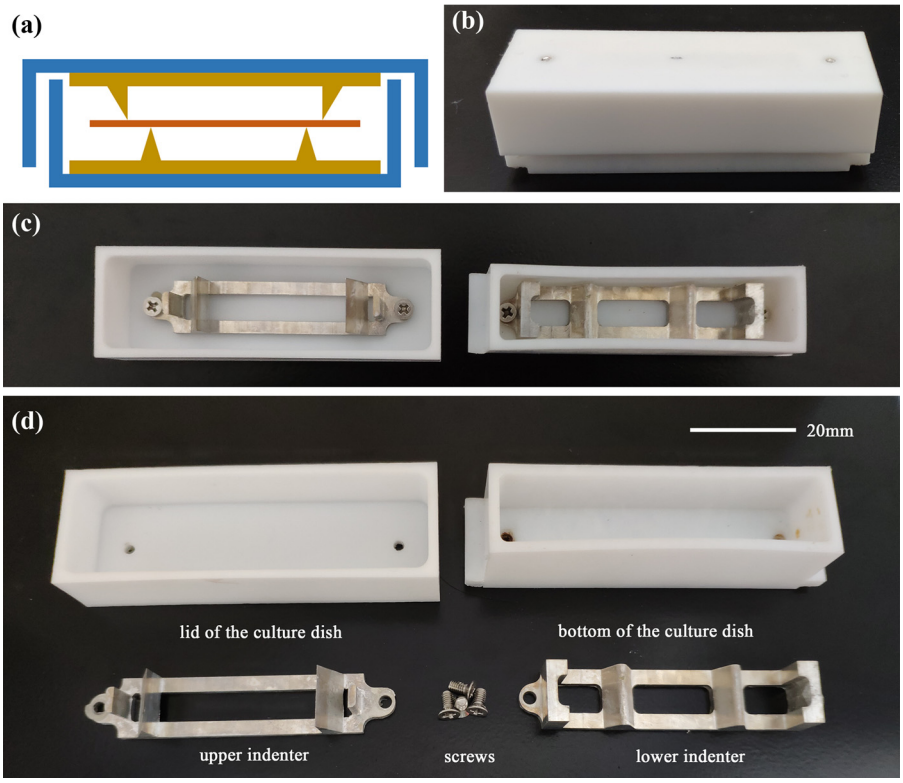

Figure 3: Schematic diagram of the four-point bending device: (a) schematic diagram of the loading process of the bone slice; (b and c) photograph of the complete four-point bending device; (d) photograph of the demounted four-point bending device.

It should be mentioned that equation (3) only provided a reference in the stage of determining the dimensions of the loading device, which could not calculate the true stress distribution in the bone slice.

2.3 Cell culture

Before the experiment, MC3T3-E1 cells were cultured in DMEM supplemented with 10% FBS (Fetal bovine serum) (Gibco, USA) in an incubator at 37°C with a humidified atmosphere of 95% air and 5% CO_2. After 80% confluence, cells were digested by 0.25% trypsin (Gibco, USA), centrifuged, and resuspended in DMEM at a concentration of 2.85×10^6 cells/mL. 5.7×10^5 cells in 200 µL cell suspension were dropped gently onto each bone slice, waiting for cell adhesion to add media till whole bone slices immersed and keep cultured for one day. Subsequently, the bone slices were divided into two groups: the stressed group and control group. Three bone slices in the stressed group were cultured in the designed loading device, and three bone slices in the control group were set at the same time. Each group was cultivated for up to 8 days. The medium was changed, collected, and stored at −80°C on day 2, 4, 6, and 8 for the later alkaline phosphatase (ALP) detection. At the end of the culture, all bone slices were harvested and stained.

2.4 Immunofluorescent observation

To make the cells visible for microscopic observation on the bone slices, cells were labeled with fluorescent dye. Each bone slice was fixed in 4% paraformaldehyde for 15 min at ambient temperature, then permeabilized with 0.1% Triton X-100 for 10 min, and blocked in 4% BSA for 30 min. The F-actin cytoskeleton of osteoblasts on bone slices was stained with TRITC Phalloidin (1:200) for 1 h, and then the cell nuclei were stained with DAPI (1:250) for 10 min. Each stained bone slice was observed under a CLSM (confocal laser scanning microscope) (Leica Microsystems, Wetzlar, Germany) at a magnification of 100-fold and the typical structures were photoed by lamellar scanning at 8 µm increments.

2.5 Cell density calculation

Due to the complexity of the microporous structures of the bone slices observed by the microscope, for better comparison, they were divided into three typical structures: the surface (S), the connection (C), and the pore wall (P), as shown in Figure 2. The surface is the surface of the bone slice, which is relatively flat; the connection is generally lower than the surface, which connects different parts of the bone slice; the pore wall consists of the wall of pores and most of the highly inclined slopes.

The photographs were then processed and classified, and typical structural images with cell distribution of all bone slices were obtained. Afterwards, Image J was used to obtain the cell density of each typical structural image, which is given by

$$\rho = \mathrm{d}N/\mathrm{d}A \tag{4}$$

where N is the number of cells on a certain structure, A is the area occupied by these cells, and ρ is the cell density on this structure.

Then the average cell density on each typical structure of the stressed and control groups was obtained, and the percentage difference η of average cell density between the two groups was expressed as

$$\eta = |(\bar{\rho}' - \bar{\rho})/\bar{\rho}| \times 100\% \tag{5}$$

where $\bar{\rho}'$, $\bar{\rho}$ are the average values of cell density of the stressed and control groups on a certain structure, respectively.

2.6 Quantitative assay of ALP activity

The viability of MC3T3-E1 cells in two groups was detected by the ALP activity in the collected medium using the colorimetric ALP detection assay kit (Mecenbio, China). First, each medium of 1 mL was freeze-dried for 24 h at a temperature of –60°C with a pressure of 0.01 mbar, and then redissolved into 160 µL of diluent (provided by the kit). Three parallel samples with a volume of 50 µL were taken from each redissolved medium and standard samples. Subsequently, the redissolved and standard samples were tested following kit instructions. Finally, the values of OD (optical density) of each sample were measured at a wavelength of 450 nm and the ALP content of each sample was obtained through OD values.

Then the average ALP content in the stressed and control groups on different days was obtained, The measured average ALP content represented the amount of ALP cell secreting within two days, which was the time interval of medium change.

2.7 Micromechanical environment analysis of the bone slice

As mentioned above, due to the complex microstructures of the bone slice, the stress state of the typical structures (S, C, and P) cells growing on was very complicated under bending moment and could not be accurately calculated. Therefore, finite element simulation was employed for the stress distribution analysis of typical structures (S, C, and P) to explore how much force was being exerted on the cells in the stressed group and provide stress data for the later model establishment.

The geometric model of the microstructures of the bone slice was created using micro-CT scanning with the accuracy of 18 µm. For further analysis, the model was improved using Geomagic Studio 2010 for smoothness. The partial model was then introduced into the Abaqus 6.13 for finite element simulation.

In Abaqus 6.13, the solid model was meshed by C3D10 elements with total grids number of 1,60,926, and a pure bending moment which was calculated according to equation (2) was applied to its cross section. The loading process was conducted using Abaqus/Standard.

2.8 Normalization of cell density in mathematical model

Due to the influence of the projection effect during the microscopic observation, cell density data were also related to structure. However, the cell density data required during the creation of the mathematical model of cell growth affected by stress must only be related to stress. Therefore the normalized technique was employed to exclude the projection effect. Since the slope structures (C and P) in the bone slices were recognized as horizontal planes under microscopic observation, the areas of these structures calculated were less than the actual areas, and the cell density values were relatively large. Therefore, the cell density values of the connection and pore wall should be normalized through dividing by a coefficient. In the control group, normalized cell density values should be the same on each structure. Therefore, the cell density values were normalized by

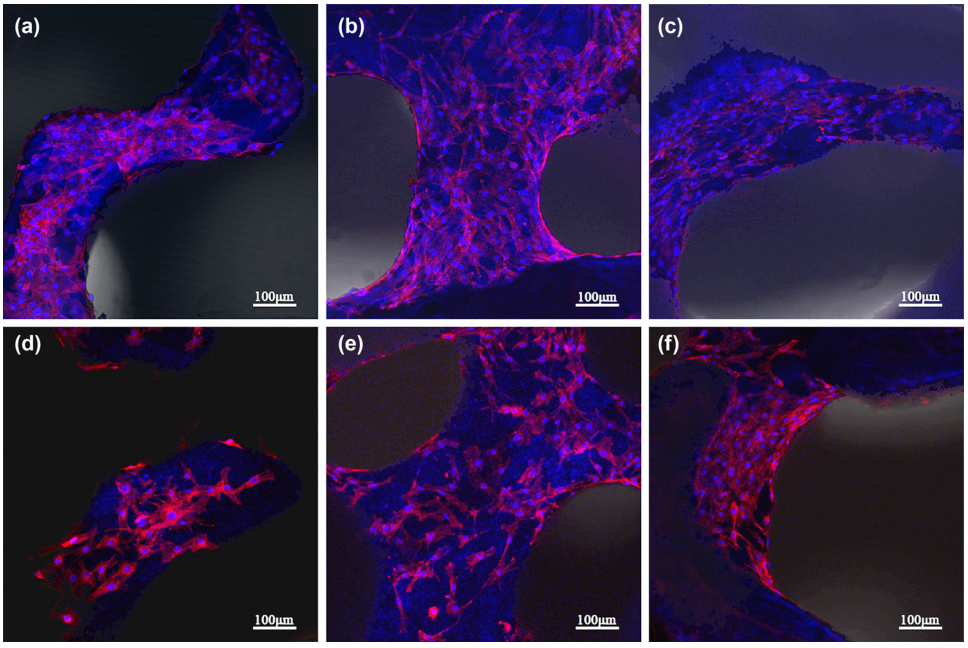

Figure 4: Cells on different typical structures in the stressed and control groups. Synthetic images of nucleus and F-actin of cells on the surface (a and d); connection (b and e); pore wall (c and f); (a–c) stressed group; (d–f) control group.

$$\rho_s/1 = \rho_c/k_1 = \rho_p/k_2 = \text{constant} \quad (6)$$

where ρ_s, ρ_c, ρ_p are average values of cell density on the surface, connection, and pore wall in the control group, respectively. k_1 and k_2 are normalization coefficients of the connection and pore wall, respectively, and they can be calculated once ρ_s, ρ_c, ρ_p are obtained from the experiment.

2.9 Statistical analysis

All values were expressed as mean ± standard deviation (SD). Statistical analysis was performed by repeated measurements analysis of variance and unpaired T test. (GraphPad Prism 8). The variance was thought to be significant when $p < 0.05$.

3 Results

3.1 Statistics and analysis of cell density

Images of cell distribution on various typical structures for the stressed and control groups are shown in Figure 4. Average values of cell density in each group and each structure were obtained, as shown in Figure 5a. The results showed that on the surface, connection, and pore wall, the average values of cell density in the stressed group were 650, 947, and 1,949 cells/mm^2, respectively, while the values were 529, 618, and 1,245 cells/mm^2 in the control group, respectively.

The average values of cell density in the stressed group were mostly higher than those in the control group. The largest difference appeared at the pore wall, reaching a value of 56.55%, followed by the connection with a value of 53.24%, and the surface had the smallest difference with a value of 22.87%. In addition, the differences were significant in the connection and pore wall between the stressed group and their relative control group. The results showed that a higher degree of proliferation occurred in the stressed group, indicating that the stress has promoted the proliferation of cells.

3.2 ALP test

Total ALP content which represented ALP content secreted by cells from the beginning to the 2nd, 4th, 6th, and 8th days was acquired through accumulating the average ALP content on different days. As shown in Figure 5b, the total ALP content in the stressed group was always a little higher

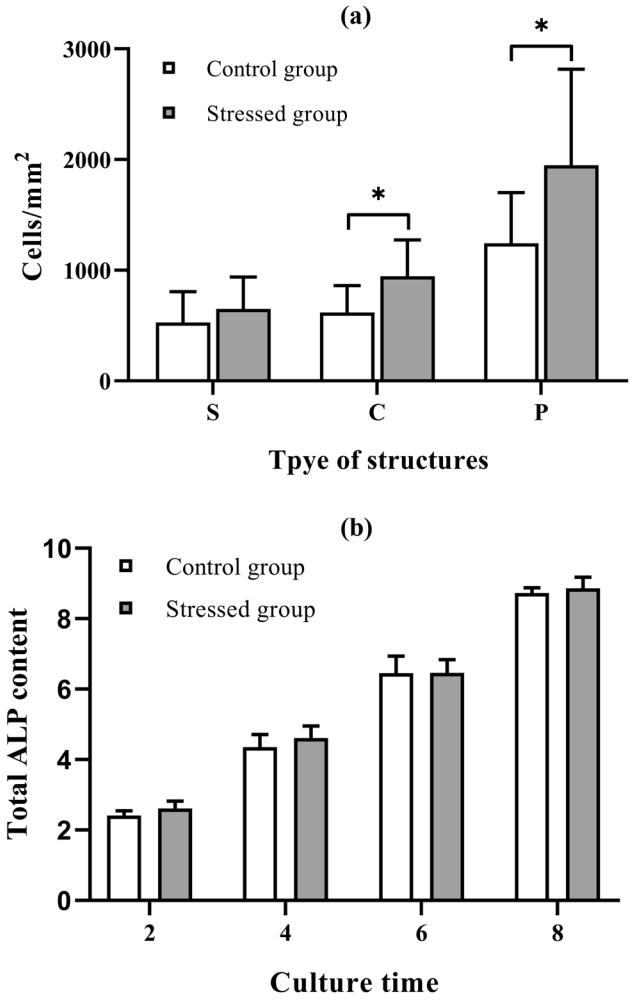

Figure 5: Results of experimental data analysis: (a) average cell density on each typical structure in the stressed and control groups; (b) total ALP content in the stressed and control groups on different days. *$p < 0.05$.

than it was in the control group. However, there were no significant differences between two groups, indicating that stress has no compelling effect on the activities of the cells. The combined results of cell density analysis and ALP test demonstrated that stress can promote the proliferation of cells while having no significant effect on the differentiation of them within the experiment duration of 8 days.

3.3 Stress of the typical structures

The distribution of Mises stress in the bone slice is demonstrated in Figure 6. Computational results showed that the micromechanical environment in the bone slice was very complicated and the stress maximum was about 84.64 kPa, while the range of stress values for the

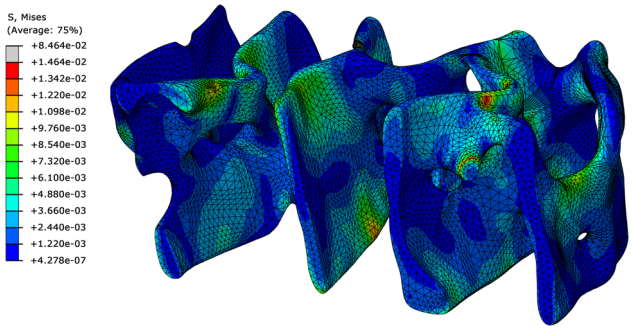

Figure 6: Mises stress distribution in the bone slice.

majority of the bone slice was 0.1–20 kPa. However, it was notable that diverse structures were experiencing different magnitudes of stress. For example, most high-stress areas were located on the pole wall. Therefore, to simplify the stress distribution, based on the typical structure division, average values of stress on each structure were calculated through 20 random points in each typical structure. The approximate average stress of the surface, connection structure, and pore wall was 2.14, 2.62, and 4.47 kPa, respectively. It can be seen that the average stress of the pore wall was the largest, followed by the connection structure, and the average stress of the surface was the smallest.

3.4 Mathematical model of cell growth affected by stress

It was significant to explore potential correlations between the stress on cells and corresponding cell density and construct a mathematical model. The first step was to obtain the correct data. It can be seen from the results of the finite element analysis that there were four stress levels in the bone slices in the experiment, which were zero of the unstressed bone slices and the average stress of the three typical structures of the stressed bone slices. According to equation (6), the normalization coefficients of the connection and pore wall were $k_1 = 1.1682$ and $k_2 = 2.3535$, respectively. All cell density values on the connection and pore wall in the stressed group were then normalized, obtaining the cell density data only relevant to stress, which is shown in Figure 7.

As shown in Figure 7, the cell density increased with the growth of stress in general, and the increasing trend gradually slowed down. This phenomenon was consistent with the theory of bone remodeling in equation (1). Therefore, based on the theory of bone remodeling, mathematical model of cell growth affected by stress was

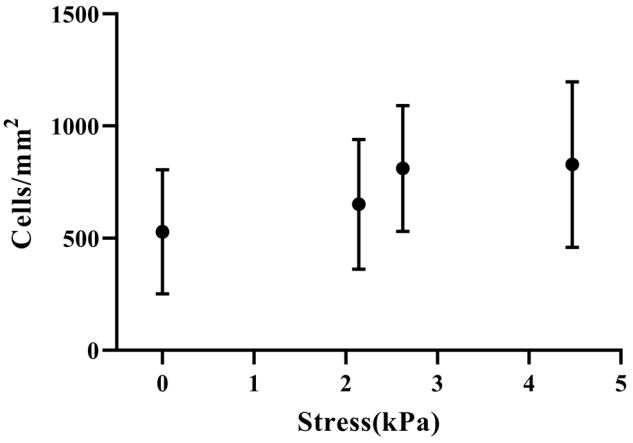

Figure 7: Cell density relationships with stress in different bone structures. The cell density values corresponding to each stress level were expressed in terms of mean and standard deviation.

established, which was given by equation (7). The average stress was an independent variable and the normalized cell density corresponding to each stress was a dependent variable.

$$\rho = \mathrm{d}N/\mathrm{d}A = a \cdot (s - 0)^2 + b \cdot (s - 0) + c \tag{7}$$

where a and b are constant coefficients, c is the density of normally growing cells without being affected by stress, s is stress, and ρ is the cell density value.

Weighted least squares estimation was used to fit unknown parameters in equation (7), because the variance of the error of each cell density value was different. Equation (7) can be expressed as

$$\rho_i = [s_i^2, s_i, 1] \cdot \begin{bmatrix} a \\ b \\ c \end{bmatrix} + v_i \tag{8}$$

where $i = 1, 2, 3, \ldots, 57$ is the sequence number of all the cell density data obtained in the experiment, and v_i is the error of ρ_i, which is assumed to satisfy a normal distribution with a mean of 0 and a variance of σ_i^2.

The covariance matrix of error v_i is

$$R = E(vv^T) = \begin{bmatrix} \sigma_1^2 & \cdots & 0 \\ \vdots & & \vdots \\ 0 & \cdots & \sigma_{57}^2 \end{bmatrix} \tag{9}$$

Equation (8) can be written in the form of a matrix as

$$y = Hx + v$$

$$\text{where } y = \begin{bmatrix} \rho_1 \\ \vdots \\ \rho_{57} \end{bmatrix}, H = \begin{bmatrix} s_1^2, & s_1, & 1 \\ \vdots & \vdots & \vdots \\ s_{57}^2, & s_{57}, & 1 \end{bmatrix}, x = \begin{bmatrix} a \\ b \\ c \end{bmatrix}, \text{ and } v = \begin{bmatrix} v_1 \\ \vdots \\ v_{57} \end{bmatrix}. \tag{10}$$

$\hat{x}$ is the best estimate of x, the residual ε_y is the difference between the measured value y and the vector $H\hat{x}$, and J is the cost function, namely

$$\varepsilon_y = y - H\hat{x} \tag{11}$$

$$J = \varepsilon_{y1}^2/\sigma_1^2 + \cdots + \varepsilon_{y57}^2/\sigma_{57}^2 \tag{12}$$

The most likely value of $\hat{x}$ was obtained when it made equation (12) the smallest. J can be expressed as

$$\begin{aligned} J &= \varepsilon_y^T R^{-1} \varepsilon^y = (y - H\hat{x})^T R^{-1} (y - H\hat{x}) \\ &= y^T R^{-1} y - \hat{x}^T H^T R^{-1} y - y^T R^{-1} H\hat{x} + \hat{x}^T H^T R^{-1} H\hat{x} \end{aligned} \tag{13}$$

$\hat{x}$ should satisfy

$$\partial J/\partial \hat{x} = -y^T R^{-1} H + \hat{x}^T H^T R^{-1} H = 0 \tag{14}$$

Therefore, $\hat{x}$ can be expressed as

$$\hat{x} = (H^T R^{-1} H)^{-1} H^T R^{-1} y \tag{15}$$

The unknown parameters were calculated by substituting relevant data into equation (15), and the result was $a = -10.0307$, $b = 116.2279$, $c = 523.2098$. The mathematical model of cell growth affected by stress can be expressed as

$$\mathrm{d}N/\mathrm{d}A = -10.0307s^2 + 116.2279s + 523.2098 \tag{16}$$

As can be seen from the model, when there is no stress present, cells proliferate at a normal rate; at this point, $s = 0$, $\rho = 523.2098$. Within the stress range of $0 < s < 11.59$ kPa, cell density values were higher than those without stress, indicating that the proliferation of cells was promoted by stress. In addition, the effect of promotion first increased and then decreased as stress increased, reaching a peak at $s = 5.79$ kPa. However, stress greater than 11.59 kPa will inhibit the proliferation of cells until excessive stress causes cell apoptosis.

4 Discussion

With the emergence of various advanced materials, many studies have tested the application effects of various biomaterial scaffolds in bone tissue engineering [34,35]. Some studies have explored the effects of stress on cells in porous scaffolds, most of which are fluid shear stresses [36–39]. However, few researchers have studied the effect of residual stress in tissue engineering scaffolds on the growth of cells, which are also very important. Therefore, in this study, the micromechanical environment of the bone slices was simulated in porous bone slices using a custom loading device, and the effect

of the micromechanical environment of porous bone slices on cell growth was studied. Furthermore, mathematical model of relationships between the cell density values and the magnitude of stress on the cells was established, which provided a quantitative method to study the effect of stress cells undergo.

The dimensions of porous materials used in previous studies are generally small. In our experiment, large bone slices were needed to apply bending moments to them, which are not easily obtained [40,41]. After many attempts, a multistep cutting method was employed to manufacture the bone slices which meet the experimental requirements, and then they were degreased and sterilized until cells can grow on them normally.

Due to the complex microstructure of the bone slices, cell distribution on them observed under CLSM was hard to analyze. In this study, a novel method was proposed to compare the difference of cell proliferation between the stressed and control groups, which have retained the complete microstructural features of the bone slices. The structures of bone slices were divided into three typical structures and cell density on these structures was compared in two groups. The results showed that the average values of cell density in the stressed group were higher than those in the control group, indicating that stress can promote the proliferation of cells. In addition, the percentage increase of cell density in the stress group reached the largest in the pore wall structure, demonstrating that cells on the pore wall structure received the most significant promotion effect. According to the results, it is recommended to increase the proportion of the pore wall structure in the microstructure design of tissue engineering scaffolds and introduce proper magnitude amount of stress to it to stimulate the proliferation of cells.

The cell activity was quantified as the amount of ALP in the collected medium. The results indicated that stress had no compelling effect on the activities of the cells. For cell differentiation, the experiment duration is not long; most cells may have not started to differentiate at the current culture time. It would be of significance to repeat this study for a longer duration and see if cell activity and osteogenic ability change over time. However, the bone slices and loading device are not easy to obtain extensively and there is an increased risk of bone slices to fracture in experimental operations as time increases.

The bone slice exposed to bending load was simulated with finite element models, and stress distribution in the microstructures of the bone slice was obtained. Results showed that different typical structures of the microstructures have different magnitude of average stress. The combined results of cell density analysis and finite element simulation reveal that higher stress causes greater promotion effect on cell proliferation.

Qualitative conclusion was drawn earlier in this article by comparing the cell density between the two groups. Furthermore, average stress of each structure and corresponding normalized cell density were used to establish the mathematical model of cell growth affected by stress. The model was fitted by weighted least square estimation which considered the measurement error variance.

This is the first time a quantitative model was established, which is able to describe the effect of complex micromechanical environment in microporous materials on cell proliferation, providing theoretical basis for tissue engineering scaffolds structure design and load application. Because the bone slices cannot bear excessive loads, the load applied to them in the experiment has not yet reached the magnitude measured in bovine femurs, and the phenomenon that excessive stress inhibits cell proliferation has not been observed. However, it was obviously found in the experiment that the rate of increase in cell density has slowed significantly as stress increases, which was very consistent with both our model and the bone remodeling theory. Based on this model, appropriate stress can be considered to be introduced into tissue engineering scaffolds during their design and manufacturing process to accelerate cell proliferation, which may accelerate the healing of bone defects.

5 Conclusion

In this study, 3D culturing experiments of MC3T3-E1 cells are performed to investigate the effect of micromechanical environment in microporous bovine bone slices on the growth of cells. The results show that stress in the bone slices promotes cell proliferation and the promotion effect is different on different typical structures. In addition, a mathematical model is established to quantitatively describe the detailed influence of stress, which provides a theoretical basis for the introduction of micromechanical environment in the bone tissue engineering scaffolds to stimulate cell proliferation and accelerate the healing process of bone defects.

Acknowledgments: This work was supported by the National Natural Science Foundation of China (Grant No. 11802010).

Conflict of interest: The authors declare no conflict of interest regarding the publication of this paper.

References

[1] Kunz F, Bergemann C, Klinkenberg E-D, Weidmann A, Lange R, Beck U, et al. A novel modular device for 3-D bone cell culture and non-destructive cell analysis. Acta Biomater. 2010;6(9):3798–807.

[2] Wu X, Stroll SI, Lantigua D, Suvarnapathaki S, Camci-Unal G. Eggshell particle-reinforced hydrogels for bone tissue engineering: an orthogonal approach. Biomater Sci. 2019;7:2675–85.

[3] Nelson ER, Huang Z, Ma T, Lindsey D, Jacobs C, Smith RL, et al. New bone formation by murine osteoprogenitor cells cultured on corticocancellous allograft bone. J Orthop Res. 2008;26(12):1660–4.

[4] Li J, Yao M, Shao Y, Yao D. The application of bio-nanotechnology in tumor diagnosis and treatment: a view. Nanotechnol Rev. 2018;7:257.

[5] Lan T, Guo Q. Phenylboronic acid-decorated polymeric nanomaterials for advanced bio-application. Nanotechnol Rev. 2019;8(1):548–61.

[6] Zang S, Chang S, Shahzad MB, Sun X, Yang H. Ceramics-based drug delivery system: a review and outlook. Rev Adv Mater Sci. 2019;58(1):82–97.

[7] Pantic S, Skodric SR, Loncar Z, Pantic I. Zinc oxide nanoparticles: Potential novel applications in cellular physiology, pathology, neurosciences and cancer research. Rev Adv Mater Sci. 2019;58(1):17–21.

[8] Langer R, Vacanti JP. Tissue engineering. Science. 1993;260(5110):920–6.

[9] Frost HM. Bone "mass" and the "mechanostat": a proposal. Anat Rec. 1987;219(1):1–9.

[10] Ellman R, Spatz J, Cloutier A, Palme R, Christiansen BA, Bouxsein ML. Partial reductions in mechanical loading yield proportional changes in bone density, bone architecture, and muscle mass. J Bone Miner Res. 2013;28(4):875–85.

[11] Sokolis DP. Strain-energy function and three-dimensional stress distribution in esophageal biomechanics. J Biomech. 2010;43(14):2753–64.

[12] Omens J, McCulloch A, Criscione J. Complex distributions of residual stress and strain in the mouse left ventricle: experimental and theoretical models. Biomech model Mechanobiol. 2003;1(4):267–77.

[13] Xu G, Bayly PV, Taber LA. Residual stress in the adult mouse brain. Biomech Model Mechanobiol. 2009;8(4):253–62.

[14] Fung YC. What are the residual stresses doing in our blood vessels? Ann Biomed Eng. 1991;19(3):237–49.

[15] Volokh K. Prediction of arterial failure based on a microstructural bi-layer fiber–matrix model with softening. J Biomech. 2008;41(2):447–53.

[16] Yamada S, Tadano S, Fujisaki K. Residual stress distribution in rabbit limb bones. J Biomech. 2011;44(7):1285–90.

[17] Yamada S, Tadano S. Residual stress around the cortical surface in bovine femoral diaphysis. J Biomech Eng. 2010;132(4):044503.

[18] Tung PK, Mudie S, Daniels JE. Hydration and radiation effects on the residual stress state of cortical bone. Acta Biomater. 2013;9(12):9503–7.

[19] Zhang Y, Nelson D. Residual stresses in bone as determined by a slotting method. Exp Mech. 2017;57(6):967–78.

[20] Hu C, Sun J, Long C, Wu L, Zhou C, Zhang X. Synthesis of nano zirconium oxide and its application in dentistry. Nanotechnol Rev. 2019;8:396–404.

[21] Kumar A, Chahal S, Hussain FSJ. Development of biomimetic electrospun polymeric biomaterials for bone tissue engineering: a review. J Biomater Sci Polym Ed. 2019;30:141308–55.

[22] Jacobs C, Grimm S, Ziebart T, Walter C, Wehrbein H. Osteogenic differentiation of periodontal fibroblasts is dependent on the strength of mechanical strain. Arch Oral Biol. 2013;58(7):896–904.

[23] Shen T, Qiu L, Chang H, Yang Y, Jian C, Xiong J, et al. Cyclic tension promotes osteogenic differentiation in human periodontal ligament stem cells. Int J Clin Exp Pathol. 2014;7(11):7872.

[24] Lim K-T, Kim J, Seonwoo H, Chang JU, Choi H, Hexiu J, et al. Enhanced osteogenesis of human alveolar bone-derived mesenchymal stem cells for tooth tissue engineering using fluid shear stress in a rocking culture method. Tissue Eng Part C Meth. 2013;19(2):128–45.

[25] Li J, Rose E, Frances D, Sun Y, You L. Effect of oscillating fluid flow stimulation on osteocyte mRNA expression. J Biomech. 2012;45(2):247–51.

[26] Koyama Y, Mitsui N, Suzuki N, Yanagisawa M, Sanuki R, Isokawa K, et al. Effect of compressive force on the expression of inflammatory cytokines and their receptors in osteoblastic Saos-2 cells. Arch Oral Biol. 2008;53(5):488–96.

[27] Baharvand H, Hashemi SM, Ashtiani SK, Farrokhi A. Differentiation of human embryonic stem cells into hepatocytes in 2D and 3D culture systems in vitro. Int J Dev Biol. 2004;50(7):645–52.

[28] Yamamoto J, Udono M, Miura S, Sekiya S, Suzuki A. Cell aggregation culture induces functional differentiation of induced hepatocyte-like cells through activation of hippo signaling. Cell Rep. 2018;25(1):183–98.

[29] Huiskes R, Weinans H, Grootenboer H, Dalstra M, Fudala B, Slooff T. Adaptive bone-remodeling theory applied to prosthetic-design analysis. J Biomech. 1987;1135–50.

[30] Weinans H, Huiskes R, Grootenboer H. The behavior of adaptive bone-remodeling simulation models. J Biomech. 1992;25(12):1425–41.

[31] Li J, Li H, Shi L, Fok AS, Ucer C, Devlin H, et al. A mathematical model for simulating the bone remodeling process under mechanical stimulus. Dental Mater. 2007;23(9):1073–8.

[32] Cullen D, Smith R, Akhter M. Time course for bone formation with long-term external mechanical loading. J Appl Physiol. 2000;88(6):1943–8.

[33] Jie Y, Li X, Cai Z, Ma M, Jin Y, Ahn DU, et al. Phosphorylation of phosvitin plays a crucial effects on the protein-induced differentiation and mineralization of osteoblastic MC3T3-E1 cells. Int J Biol Macromol. 2018;118:1848–54.

[34] Xie X, Zhang Q, Zhou T, Ma Q, JinFeng L. The review of nanomaterials inducing the differentiation of stem cells into chondrocyte phenotypes in cartilage tissue engineering. Curr Stem Cell Res Ther. 2018;13:7.

[35] Cheng H, Hu H, Li G, Zhang M, Xiang K, Zhu Z, et al. Calcium titanate micro-sheets scaffold for improved cell viability and osteogenesis. Chem Eng J. 2020;389:124400.
[36] Bancroft GN, Sikavitsas VI, van den Dolder J, Sheffield TL, Ambrose CG, Jansen JA, et al. Fluid flow increases mineralized matrix deposition in 3D perfusion culture of marrow stromal osteoblasts in a dose-dependent manner. Proc Natl Acad Sci U S A. 2002;99(20):12600–5.
[37] Sikavitsas VI, Bancroft GN, Holtorf HL, Jansen JA, Mikos AG. Mineralized matrix deposition by marrow stromal osteoblasts in 3D perfusion culture increases with increasing fluid shear forces. Proc Natl Acad Sci U S A. 2003;100(25):14683–8.
[38] Rumney R, Sunters A, Reilly G, Gartland A. Application of multiple forms of mechanical loading to human osteoblasts reveals increased ATP release in response to fluid flow in 3D cultures and differential regulation of immediate early genes. J Biomech. 2012;45(3):549–54.
[39] Jia Y-Y, Li F, Geng N, Gong P, Huang S-J, Meng L-X, et al. Fluid flow modulates the expression of genes involved in the Wnt signaling pathway in osteoblasts in 3D culture conditions. Int J Mol Med. 2014;33(5):1282–8.
[40] Anselme K, Noel B, Flautre B, Blary M-C, Delecourt C, Descamps M, et al. Association of porous hydroxyapatite and bone marrow cells for bone regeneration. Bone. 1999;25(2):51S–4S.
[41] Açil Y, Terheyden H, Dunsche A, Fleiner B, Jepsen S. Three-dimensional cultivation of human osteoblast-like cells on highly porous natural bone mineral. J Biomed Mater Res. 2000;51(4):703–10.